Parallel Simulations of Reacting Two-Phase Flows: A DoD Grand Challenge Progress Report*

S. Menon†, S. Pannala‡, W.-W. Kim††, T. M. Smith‡‡ and S. Arunajatesan†††
School of Aerospace Engineering
Georgia Institute of Technology
Atlanta, GA 30332-0150

Abstract

Parallel simulation of unsteady turbulent combustion is carried out for a range of precursor test problems leading to the development of a new methodology for reacting two-phase flows. Simulations are carried out using large-eddy simulations (LES) which allows full spatio-temporal resolution of all scales larger than the grid resolution with the unresolved small-scales modeled by a localized dynamic one-equation subgrid models. For two-phase applications, Lagrangian tracking of a range of droplets is carried out and is fully coupled to the Eulerian gas phase flow. An extension of this approach to accurately deal with small-scale scalar mixing and chemical reactions has been carried out using an innovative model that is implemented within each LES cell, to account for the effects of small-scale mixing and molecular diffusion on the chemical processes. The first year's effort focused on validating this methodology using both simple and complex test configurations. Highly optimized parallel LES codes are used for these studies. In addition to parallel scaleup data, results discussed in this paper include stagnation point premixed flame, opposed jet diffusion flame, highly swirling premixed flame in a General Electric combustor and two-phase mixing and vaporization in mixing layers. Comparison with experimental data wherever possible, clearly demonstrates the unique capabilities of the new subgrid combustion LES model.

Introduction

Most practical combustion systems as in gas turbine engines, internal combustion engines, liquid-fueled rockets, etc., employ liquid fuel and gaseous oxidizer for the combustion process. As a result, many physical processes (such as liquid jet breakup, atomization, droplet vaporization, and fuel-air mixing) occur prior to the actual combustion process. The heat released during combustion in turn will modify the turbulence in the flow resulting in a fully coupled evolution of the fluid flow and chemical processes. All these processes are highly unsteady and in most real systems, occur in a highly turbulent environment. Current understanding of this type of flow field is severely limited and comes primarily from experiments carried out using simplified test configurations. Future advancement in engine design and increase in efficiency (i.e., reduced fuel consumption and pollutant emission) will require a more in-depth understanding of the combustion processes. However, experimental studies of real combustors are difficult primarily because of the difficulty in accessing the reaction zone with non-intrusive instruments. Furthermore, diagnostic tools currently available can only provide information on only a few species and in most cases, can provide only limited information on the dynamics of the processes. In addition, parametric experiments on complex real engines can easily become prohibitively expensive.

An alternate method would be to employ numerical methods since they are more cost effective. However, at present there are no modeling tools available to address this type of unsteady flow primarily due to (a) the lack of physically accurate models and (b) the lack of adequate computing resources. With the availability of massively parallel systems under the DOD HPC Grand Challenge Project and the recent development of a physically accurate simulation model (discussed in this paper), these limitations can be relaxed to some extent so that it becomes feasible to address simulation of high Reynolds number reacting, turbulent, two-phase flows. However, it is worth noting here that in spite of the recent development of parallel systems with terraflop capability, simulations of such flows in practical systems are still considered impossible since both the memory and processing speed requirements are far beyond the current capability. However, the

†. Professor, Senior Member AIAA
‡. GRA, Student Member AIAA
††. Post Doctoral Fellow, Member AIAA
‡‡. Currently at Sandia National Laboratories, Albuquerque; Member AIAA
†††. GRA, Student Member AIAA

development and validation of a physically accurate method of simulation using current facilities will go a long way towards establishing a viable tool for simulating such complex flows in the future when picaflop machines become available. This paper reports on the development of such a simulation tool. It is also shown here that this development requires the availability of parallel processing systems both due to the nature of the model and due to the processing power needed to evaluate the model's performance.

Simulation Model

The present research is focussed on improving the liquid fuel atomization process and to increase fuel-air mixing downstream of the fuel injector in advanced gas turbine combustors. Since fuel atomization and fuel-air mixing are both highly unsteady, conventional steady state methods cannot be used to elucidate the finer details. On the other hand, although unsteady mixing processes can be studied quite accurately using direct numerical simulation (DNS) (e.g., Poinsot, 1996), application of DNS is limited to low to moderate Reynolds numbers (Re) due to resolution requirements and therefore, cannot be used for high Re flows of current interest.

The present study employs the technique of large-eddy simulations (LES). In LES, the scales larger than the grid are computed using a time- and space-accurate scheme, while the unresolved smaller scales are modeled. The Navier-Stokes equations that govern the conservation of mass, momentum and energy in a fluid are filtered to obtain the LES equations. The filtering operation results in terms in these equations that must be modeled. Closure of momentum and energy transport equations can be achieved using a subgrid eddy viscosity model since the small scales primarily provide a dissipative mechanism for the energy transferred from the large scales. A local dynamic model for the subgrid turbulent kinetic energy has been developed for the closure of the subgrid terms in the momentum and energy equations (Kim and Menon, 1995; Menon and Kim, 1996; Nelson and Menon, 1998). Application of this subgrid model in turbulent flows shows that this model is capable of accurately representing the effect of unresolved terms even when relatively coarse grids are employed. The details of the LES equations and the subgrid closure employed have been reported in the cited papers and therefore, are avoided here for brevity.

Subgrid closure of this manner (i.e., based on an eddy viscosity model) cannot be used for modeling the scalar transport since for combustion to occur, the species must first mix at the molecular level. The small scales of motion control this stage of mixing, which are typically unresolved in LES. Thus, ad hoc models for the subgrid (unresolved) scales cannot be used.

To address these issues, recently (Menon et al., 1993; Menon and Calhoon, 1996; Calhoon and Menon, 1996, 1997; Smith and Menon, 1998), a subgrid combustion model was developed and implemented within the LES formulation. This model separately and simultaneously treats the physical processes of molecular diffusion and small scale turbulent convective stirring. This is in contrast to probability density function closure which phenomenologically treats these two processes by a single model, thereby removing experimentally observed Schmidt number variation of the flow.

In the approach developed at Georgia Tech called LES/LEM, the resolved scale mass, momentum, and energy transport are simulated on a conventional grid using a conventional LES method. However, no scalar transport is simulated on the LES grid. Rather, within each LES cell, a subgrid one-dimensional (1D) domain is defined and within this 1D domain, turbulent small-scale mixing, molecular transport and chemical kinetics are explicitly modeled. The local 1D domain can be visualized as a stochastic instantaneous slice of the local 3D flame brush and the resolution in this domain is chosen to resolve all relevant length scales. As a result, the chemical reaction-diffusion equations can be solved without any assumptions (i.e., as a direct simulation). This model requires that all the local time scales associated with each of the small-scale processes must be resolved. Therefore, in each grid cell, a significant amount of computations must be carried out in-between the large-scale (LES resolved) time step. Therefore, this model is uniquely suited for parallel processing and has been implemented on various systems such as: CRAY T3E and SGI PC/Origin 2000 using system independent Message Passing Interface (MPI) compiler.

The gas-phase methodology was recently extended to two-phase flows (Menon and Pannala, 1997) to capture accurately the process of phase change and turbulent mixing. The method has also been further refined and used to study vaporization and the subsequent chemical reactions. Both infinite and finite-rate kinetics have been investigated (Pannala and Menon, 1998).

The two-phase simulation model is part of a suite of simulation codes developed at the Computational Combustion Laboratory in Georgia Tech. These codes (of increasing complexity and applicability) have been used to methodically develop the new subgrid combustion simulation approach. As noted earlier, the goal of these studies is to develop and validate a scheme that can be used to investigate and design the next generation gas turbine engines. The present methodology is computationally much more expensive when compared to codes currently being employed. However, the potential increase in accuracy and the projected ability of the new approach to capture complex phenomena and radical kinetics justifies the added expense. Furthermore, with the increase in computational power, such intensive calculations may become acceptable in the future especially when even more massively parallel systems (i.e., with processors > 1000 CPU's) become available. Therefore, the current development effort is directed towards a longer-term

goal of developing a more fundamentally accurate and physically consistent simulation tool to address future gas turbine concerns.

The present approach combines features of both Eulerian-Eulerian (gas-liquid) and Eulerian-Lagrangian (gas-liquid) modeling approaches. In this approach, gas phase calculations are carried out using an Eulerian large-eddy simulation (LES) method while the liquid droplets are tracked within the Eulerian gas phase using a Lagrangian particle tracking method. The droplets are integrated in time in each of the gas phase LES cells and are transported across the Eulerian domain. In this process, the droplets exchange mass, momentum and energy with the local gas phase. In conventional two-phase modeling, all droplets smaller than a prespecified cut-off size are assumed to instantaneously vaporize and mix. However, results have confirmed that this assumption is highly erroneous unless the cutoff size is very small. Increasing the cutoff size without sacrificing accuracy is of great interest since this would reduce the computational time significantly. Therefore, in the present model, this issue has been addressed such that the droplets below the cut-off are carried into the subgrid using a void fraction Eulerian formulation to simulate the effect of droplets all the way till the liquid phase completely vaporizes and mixes at the smallest scales. Again, for brevity, the details of the formulation and the representative equations are avoided here. Details are available in the cited papers (Menon and Pannala, 1997; Pannala and Menon, 1998).

Parallel Implementation

The technique of data concurrency (i.e., the primary data space is partitioned and distributed among the processors) rather than functional concurrency (i.e., the overall application is decomposed into several distinct parallel computational tasks) was chosen after careful review of the type and degree of parallelism inherent in the numerical algorithm used for LES. The data space is partitioned and distributed to the processors so that 1) the distribution of cells to the nodes leads to a nearly balanced load of communication and computation among all nodes, and 2) the inherent spatial data locality of the underlying cell structure is maintained so as to minimize interprocessor communication. The cell-partitioning scheme decomposes the 2D (3D) computational domain into logically congruent, nearly equal-sized rectangles (cubes). Maximum concurrency is extracted to minimize the execution time on a given number of processors. The overheads associated with parallel implementation, such as, (1) load imbalance, (2) inter-processor communication, (3) data dependency delays, (4) arithmetic, and (5) memory, were analyzed. While the first four types of overheads lead to performance degradation, the memory overhead limits the size of the problem that can be executed on a fixed number of processors. In practice, simultaneously minimizing all these overheads is very difficult.

In the present implementation, the partitioning scheme results in each processor performing computations only on the cells held by it. For finite-difference or finite-volume schemes, each domain contains extra layers of ghost cells along the processor partitions to allow the exchange of boundary cell data. This exchange is carried out using a few relatively long messages. As a result, the high cost of latency associated with message passing is minimized, resulting in a reduced communication overhead even though this data exchange results in an increased memory overhead.

The implementation of the subgrid combustion model within the LES method is relatively straightforward since the subgrid model resides within the LES cells and requires no inter-cell communication for the local subgrid processes. However, inter-processor communication is needed every LES time step to transport the subgrid scalar field across LES cell surfaces. These messages carry the local scalar information. However, unlike the long messages needed for the fluid dynamics part, these messages are from the nearest neighbor cells and thus, are relatively short messages.

The current implementation on parallel systems employs double precision (64-bit) arithmetic and is based entirely on FORTRAN. Performance comparison with and without I/O has been carried out. However, I/O overhead is unavoidable since the data generated on the spatio-temporal evolution of the flow field is needed for analysis. The type, form and frequency of data vary with the problem and thus, cannot be standardized. In general, the 3D flow fields are needed for flow visualization and for restart files. The present approach combines both these requirements by making all processors to write the required data into one file. The location of this file depends on system architecture: The file can reside either on the local file system (T3D & T3E) or it has to reside on one processor (e.g. IBM SP2). To optimize I/O time on all systems, the flow variables from all processors are written one at a time into a temporary buffer array which always resides on one processor, and then this array is written to a file. This approach results in one processor writing a large amount of data instead of all processors writing small amounts of data (which was found to cause I/O bottleneck). This I/O implementation works quite well on all systems used here and is considered an optimal compromise to allow flexibility in porting the code (and data) to different systems. In addition, this approach allows the simulation to be restarted on arbitrary number of processors. This capability is very useful when the system is heavily loaded. A disadvantage of this approach is that a large buffer array is needed (on one processor) which again results in an increased memory overhead and limits the memory available for the simulation on each node.

Some timing data is reported here to demonstrate the scalability and efficiency of the parallel simulations codes developed at Georgia Tech. Figure 1 shows the typical scaling of the axisymmetric and 3D codes on various systems. The direct simulation (DNS) timing is

less than the LES timing because the latter solves an additional equation for the subgrid kinetic energy. However, LES are usually performed using much coarser grids and therefore, are relatively, computationally less intensive. On the systems shown in these figures, these codes show nearly linear scaleup when the number of processors are doubled. In general, among the distributed processing systems examined here, the SP2 is the fastest for all test cases. However, for a fixed grid size, as the number of processors is increased, the scaleup is superior on both T3D and the Paragon. Also shown is some data obtained on the mixed shared/distributed-memory SGI-PC (MIPS 8000/75 MHz) system (using the same code and MPI). Results suggest that for the same number of processors used, the SGI-PC performs the best (and is twice as fast as the SP-2). For comparison, on a single processor Cray C90, a vectorized version of the 3D code executes at around 487 MFLOPS and requires 0.95 sec per iteration (equivalent to 64- processors SP2).

Figures 2a and 2b show the timing data for the subgrid combustion model obtained on a number of older systems. For a fixed LES resolution, increasing the subgrid cells increases the CPU time. However, the scale-up is still very good and nearly linear (Fig. 2a). Of particular interest is the slow increase in CPU time on a fixed number of processors (Fig. 2b) with increase in the subgrid resolution. Results show that when the subgrid resolution is increased by a factor of 2, the CPU time (on T3D) only goes up by around 30%; when the resolution is increased by a factor of 5, the time increases by around 2.0. This is due to the increase in local computations relative to the communication overheads. The T3D and SP2 timings are quite close while on the C90 the execution time is increased by 78% when the resolution is doubled. This clearly demonstrates that the combustion subgrid model is much more efficient (more than a factor of 2) on the parallel systems.

The above timing studies were repeated on the newer machines, the SGI Origin 2000 and the CRAY T3E. The results of the scale-up are summarized below.

Table 1 summarizes the various execution timings for the 2D code on more recent machines: the CRAY T3E, and Origin 2000. For comparison, the T3E data is used as a reference and the other data are normalized using the T3E data. As a further reference, we have also included data obtained on a Pentium II (300 MHz) cluster (IHPC) which was simply built using off-the-shelf PCs and 100 Mbit per second switched Ethernet connection. Clearly, this code is highly scalable and achieves over 60% in efficiency on all the DoD systems. It is interesting to note that both the communication and compute speed of the Origin 2000 is much better than the T3E for the same number of processors studied. Our experience suggests that the scale-up is still quite good on the T3E when a large number of processors (>100) are used (note that the Origin 2000 is not available in that size for simulations). Another interesting point to note here is that the Pentium II cluster is only a factor of 2 slower than the T3E for computations using 32 processors. However, our more recent studies on the IHPC cluster show that the Pentium cluster does not scale-up efficiently when the number of processors are increased beyond 32. Note that these studies did not include I/O times. If I/O was included, the IHPC cluster becomes quite inefficient.

The timing data for the 3D LES code is summarized above in Table 2 for the T3E and the Origin 2000. The 3D code achieves 32.33 Mflops per processor on 90 processors. This compares very well with some parallel benchmarks. The data shows that the 3D code also achieves very high scale-up efficiency on the newer machines. This efficiency is critical since full 3D LES can be quite expensive. For example, using 1 million grid points, a 3D conventional LES (i.e., without the subgrid combustion model) with a thin flame model (results from this approach are discussed in the next section) requires over 20000 single-processor hours on the Cray T3E, for sufficient data for statistical analysis. In real time, using 256 processors, this type of large-scale simulation is still feasible on current machines. When the subgrid combustion model is included, the computational cost can easily double. Thus, high scalability of simulation codes is essential for the studies envisioned using the new simulation approach and therefore, considerable amount of effort has been expended over the last few years to develop efficient simulation codes.

Results and Discussion

The development of the two-phase LES model requires implementation and validation of various submodels before the final product can be utilized for practical simulations. The validation of these various submodels are the basis of current research and are discussed below.

Four different test problems are discussed below. The first two configurations - opposed jet diffusion flame and the stagnation point flame - are building block problems that have been experimentally studied extensively. Thus, there is a large amount of data available for comparison and for validation. Turbulent flow simulations in these configurations summarized here and described in more detail elsewhere (Smith and Menon, 1998) are the first such studies to be reported. The results obtained so far clearly validate the accuracy and the capability of our baseline LES code.

The third configuration is an actual premixed swirling combustor (General Electric's LM6000) under realistic conditions. Comparison with data demonstrates the validity of our LES approach. Finally, the fourth problem deals with the two-phase mixing and vaporization in mixing layers using both conventional and the new subgrid approach. The validation reported here and elsewhere (Menon and Pannala, 1997; Pannala and Menon, 1998) serves to establish this LES methodology and sets the stage for more complex flow simulations planned for the next year.

LES of Opposed Jet Diffusion Flames

Opposite jet diffusion flame has been investigated experimentally for quite some time and is a well-characterized diffusion flame problem that can be used to evaluate simulation models. The key feature of this configuration is shown schematically in Fig. 3. Two streams (fuel and oxidizer) impinge upon each other. Fuel-air mixing occurs near the impingement region. Once ignited, a diffusion flame will exist wherever the mixture is stoichiometric. By changing the jet speeds, it is possible to incorporate the effect of strain on the diffusion flame. Experimental studies of this configuration have been carried out under both laminar and turbulent conditions. However, numerical studies have been limited to only laminar flows or steady-state turbulent flows, since it has been quite difficult to simulate unsteady turbulent conditions. Recently, unsteady simulations of this configuration for turbulent conditions were successfully carried out. Turbulence at a specified intensity level and with an appropriate spectrum is introduced into the computational domain from the inflow. The resulting vortices in the flow field interact with the reaction zone to wrinkle the flame region. We expect to report the detailed analysis of these calculations in near future.

Typical simulations were carried out using 64 processors on the Cray T3E and required 1.7 GB of RAM and 5000 single processor hours to obtain sufficient data for validation (12 flow through times). Figure 4 shows a typical result of the simulation. The effect of turbulence on the flame region can be clearly seen. It can be observed that the turbulent eddies (vortices) wrinkle the flame structure from both sides. Both large and small-scale wrinkling of the flame can be seen. This is consistent with experimental data.

LES of Stagnation Point Premixed Flames

Stagnation point flames have also been studied experimentally for quite some time since it forms a fundamentally clean problem to isolate the effects of turbulence-chemistry interaction on premixed flames. In Fig. 3 if a wall replaces the centerline plane and a premixed fuel-air mixture replaces the fuel or air stream, one would obtain the stagnation point configuration. A fundamental advantage of this configuration is that nearly stationary premixed flame is obtained and therefore, the flow-chemistry interactions can be analyzed in detail. Figure 5a shows the typical flame structure in the current LES approach with the subgrid combustion model and Fig. 5b shows a typical visualization of a similar flame in the experiments (Cheng, 1991). Clearly, the effect of turbulence is to wrinkle the flame and these results in both large and small-scale wrinkles in the flame structure. Both the experimental and numerical results show similar results. Figure 6 shows the effect of the vortices in the turbulent stream is to cause the observed wrinkles in the flame. Although both the opposed jet diffusion flame and the stagnation point flame qualitatively look quite similar, there are many obvious, as well as, subtle differences between the two types of flames which are discussed elsewhere.

Further comparisons, of the present calculations against experimental data on the predicted turbulent flame speed (Smith and Menon, 1998) clearly show that the present approach has achieved a reasonably good agreement with the data. For example, in Fig. 6b normalized turbulent speed is plotted against turbulent intensity. These two-dimensional simulations compare very well with the data from Cho *et al.*, 1996 but underpredict the data of Liu and Lenze, 1988. The discrepancy with the latter set of data may be due to some differences in the experimental setup that is not captured by the present simulations. In addition, the two high S_L correlations of Liu and Lenze contain significant amounts of hydrogen in the reactant mixtures in order to increase S_L. This presence of hydrogen reduces the Lewis number so that the turbulence increases the turbulent flame speed by a greater amount than in the case of pure methane where the Lewis number is close to unity. Note that this type of agreement has never been achieved in the past since no simulation model has been able to simulate this type of flow. The present study is the first known simulation of turbulent premixed stagnation point flame. Comparison with data clearly demonstrates the potential of the scheme.

Typical simulation using 20,000 grid points with 70 subgrid cells on the Cray T3E required around 2 GB of memory and 5000 single processor hours to obtain sufficient data for analysis (around 10 flow through times).

LES of Highly Swirling Premixed Flames

General Electric's lean premixed dry low NOx emissions LM6000 gas turbine combustor has been simulated. As shown in Fig. 7, this problem has a complicated geometry. A highly swirling jet (the maximum value of tangential velocity component is slightly greater than the peak value of axial velocity component) is injected from a circular inlet under high pressure ($P=6.18\times10^5$ N/m^2 ~ 6 atmospheres) and temperature (T=644 K) conditions. The combustor comprises of a rectangular box with two blocks located at top and bottom surfaces from which cooling air is blown downstream. The present simulation of the flow was implemented using state-of-the-art turbulent combustion models. This method employed the G-equation turbulent flamelet model (Kerstein et al., 1988) based on Pocheau's turbulent flame speed model (Pocheau, 1994) and localized dynamic k-equation subgrid-scale turbulence model (Menon and Kim, 1996; Nelson and Menon, 1998). The typical maximum inflow axial jet velocity is 100m/s and the Reynolds number based on the maximum velocity is 350,000. LES was carried out using 300,000 and 500,000 grid points.

Time averaged vorticity magnitude

$(|\omega| = \sqrt{\left(\frac{\partial u}{\partial z}-\frac{\partial w}{\partial x}\right)^2+\left(\frac{\partial v}{\partial x}-\frac{\partial u}{\partial y}\right)^2+\left(\frac{\partial w}{\partial y}-\frac{\partial v}{\partial z}\right)^2}$ where u, v and w are the streamwise, normal and spanwise components of the velocities) contour plots are shown in Figs. 8 (a-d) while two arbitrarily chosen instantaneous vorticity fields are shown in Figs. 9 (a-d) and Figs. 10 (a-d). The plots include one plane perpendicular to z-axis through the combustor centerline and three planes perpendicular to x-axis at three different down stream locations of the inlet (x=6 mm, 24 mm, and 78 mm, respectively). The swirling incoming premixed jet expands rapidly and results in a forward stagnation point. The unsteadiness of the flow can be clearly seen in the plots (see Figs. 9 and 10). Figure 11 shows the time averaged (a) and instantaneous (b&c) flame kernel. The unsteadiness of the combustion process and the flame kernel can be easily noted by contrasting Figs. 11 (a, b&c).

Figure 12 shows a comparison of the predicted velocities with experimental data. The axial velocity comparison is shown along the combustor centerline (Fig. 12a) and along y-axis at x=6 mm downstream of the inlet (Fig.12b). The agreement is considered quite satisfactory. Similar agreement is also observed for the other components of velocity and at other locations where data was available. Some typical comparisons are presented on Fig. 12c (comparison of the radial velocity along y-axis at x=24 mm) and Fig. 12d (comparison of the tangential velocity along z-axis at x=24 mm) to demonstrate the ability of this simulation.

A typical simulation using 500,000 grid points on the CRAY T3E required around 2.2 GB of Memory and 22,000 single processor hours to obtain sufficient data for statistical analysis (20 flow through times).

LES of Two-Phase Flows in Mixing Layers

The two-phase subgrid model was first implemented into a 3D zero-Mach number code developed earlier (Chakravarthy and Menon, 1997). Briefly, this code solves the LES equations on a non-staggered grid. Time integration employs a two-step semi-implicit fractional step method that is second-order accurate. The spatial difference scheme is fifth-order for the convective terms and fourth-order for the viscous term. The Poisson equation for pressure is solved numerically using a second-order accurate elliptic solver that uses a four-level multigrid scheme to converge the solution. The Lagrangian tracking of the droplets is carried out using a fourth-order Runge-Kutta scheme. More details of the schematic are given in Menon and Pannala (1997) and Pannala and Menon (1998).

Before simulating reacting flows, an attempt was made to validate the Lagrangian approach of particle tracking. Although quantitative comparison with earlier studies is difficult due to differences in the set up and/or initial conditions, qualitative comparison can be carried out. For this purpose, we simulated the mixing layer studied by Lazaro and Lasheras (1992a,b) and simulated by Martin and Meiburg (1994) using a 2D vortex method. Here we employed a 3D approach and simulated a temporal mixing layer on a 64x64x64 grid. The particles were injected in every cell of the upper stream with zero velocity. The total number of particles tracked is 65,500. This case is very similar (except for the differences in grid resolution and the number of particles employed) to the direct simulation of Martin and Meiburg (1994). Particle dispersion was computed for a range of Stokes numbers. Here, the Stokes number is defined as: $St = \frac{\rho_p d_p^2}{18\mu}\cdot\frac{\nabla U}{\delta_\omega}$, where δ_ω is the vorticity thickness and ∇U is the velocity difference between the upper and lower stream.

Figure 13a shows the dispersion of particles (in terms of the dispersion thickness) with time for a range of Stokes numbers. Also, the 0.9-0.1 level thickness (δ_L) is the difference between the cross-stream locations where the particle concentration is 90% and 10% of the reference value, respectively. It can be seen that the dispersion of particles of order St=1 exceeds that of droplets with St<1 (i.e., smaller droplets). This phenomena was observed earlier in both experimental (Lazaro and Lasheras, 1992b) and numerical (Martin and Meiburg, 1994) studies and was attributed to the increased lateral dispersion of the particles when the aerodynamic response time is of the order of the characteristic flow time. The present result agrees with these earlier results. The increased particle dispersion leads to the formation of streaks for particles for St=5 as shown in Fig. 13b. This agrees qualitatively very well with the experimental observations of Lazaro and Lasheras, 1992b (Fig. 13c). Note that the gray scale figure gives the false appearance that there are more particles in the lower stream but that is only an aberration of the image.

In the following, the discussion focuses primarily on comparing the subgrid model with the conventional model (other details are given elsewhere - Menon and Pannala, 1997; Pannala and Menon, 1998). For these studies, droplets were injected into the core of the mixing layer at time t=0. The mixing layer is initialized by a tangent hyperbolic mean velocity along with the most unstable 2D (of dimensional wavelength 2π) mode and random turbulence (similar to that described in Metcalfe et al., 1987). Results shown here employed a grid resolution of 32x32x32. Grid independence studies were also carried out for some of these cases using a 64x64x64 grid and good agreement was obtained.

The mixing layer is initialized with the oxidizer in both the upper and lower streams at 350 K and the fuel droplets are initially introduced in the mid-plane. Droplets in 10-50 micron radius range with an initial temperature of 300 K were used for all simulations with the droplet cutoff radius at 5 micron. A total of 2100 droplet groups are tracked. For simplicity, the droplet groups were uniformly distributed and the number of

droplets in each group is chosen such that the overall mass loading is 0.5 and the corresponding volume loading is 0.0005.

Figure 14a shows the spanwise vorticity ($\omega_z = \left(\frac{\partial v}{\partial x} - \frac{\partial u}{\partial y}\right)$, where u and v are the streamwise and normal velocity components respectively) contours in the mixing layer at the roll-up stage for a case in which the particles are passively transported upon insertion (i.e., no vaporization included and hence, there is no coupling between the two phases). It can be seen that the shear layer rolls into coherent structures as seen in pure gas phase flows. However, when droplet vaporization is included, as shown in Fig. 14b, the associated heat absorption results in major changes in the shear layer. The formation of the coherent spanwise vortices is inhibited due to vaporization (and mass addition to gas phase). Although the extent of the mixing layer appears to be large, the peak value of the spanwise vorticity is substantially lower for the vaporizing case. Analysis shows that, in the vaporization case, significant 3D vorticity is generated and this plays a major role in inhibiting the spanwise coherence.

The enhancement of streamwise vorticity ($\omega_x = \left(\frac{\partial w}{\partial y} - \frac{\partial v}{\partial z}\right)$, where v and w are the normal and lateral velocity components respectively) can be visualized by comparing Figs. 15a and 15b which show, respectively the streamwise vorticity for the passive and vaporization cases. The 3D nature of the shear layer has been enhanced in the vaporization case (notice that the same contour interval is employed for direct comparison). Further analysis shows that vaporization causes significant production of the baroclinic torque outside the vortex core. This production plays a major role in redistributing the vorticity in the mixing layer. This can be confirmed by calculating the various terms in the 3D vorticity transport equation and details have been reported in Pannala and Menon, 1998. The droplet distribution for the two cases shows that the droplets follow the fluid motion and this behavior qualitatively agrees with the results obtained by Ling et al. (1997). Differences exist due to modulation of the vortex structures as a result of vaporization (as noted above).

The spanwise and streamwise vorticity for the subgrid approach are shown in Figs. 16a and 16b, respectively and correspond to Figs. 14b and 15b for the conventional case. The effect of vaporization on shear layer is qualitatively similar in nature but the magnitude is much higher for the subgrid approach. This can be explained by noting that in the LEM approach phase change occurs in the subgrid and more details of fine scale mixing effects are included.

Note that in the subgrid case, if the droplet cutoff is chosen such that no droplet drops below the cutoff, then the void fraction is zero. In this case, the subgrid and the conventional approaches should agree reasonably well. This has been confirmed using infinite kinetics when the vaporized fuel mixes with the oxidizer and instantaneously reacts. The product mass fraction (ratio of the product density to the overall gas density) predicted by the conventional and the subgrid approaches are compared in Fig. 17a. It can be seen that there is very good agreement thereby confirming the validity of the subgrid approach. The predicted temperature of the gas phase (Fig. 17b) also shows good agreement.

If the cut-off size is large, then the conventional LES will be in significant error since it assumes that all droplets below cut-off instantaneously vaporizes. However, if the new subgrid approach can deal with this increased cut-off size (by the subgrid void fraction approach) then it will reduce the computational cost of the Lagrangian tracking considerably. To determine this, two cut-off sizes of 10 and 20 microns were used in otherwise identical simulations. In order to retain the droplet information into the subgrid, the droplet size is chosen from a realistic distribution between the cutoff and the lowest possible droplet size. The number of bins chosen varies with the cutoff radius. Currently, the liquid void fraction is passively transported across LES cells based on the volume transfer of the gas phase and this might lead to some convection errors. However, the liquid phase transport should be based on the liquid volume transfer from the LES cell. A method to deal with this transport has been developed and will be used in future studies.

The product mass fraction obtained by the two different LES methods are compared in Figs. 18a and18b, respectively, for the various cut-off sizes. The results predicted by the conventional LES are in gross error for cut-off radius of 10 and 20 micron. However, the present methodology agrees very well over the cutoff range. Ideally, the subgrid model should predict identical results for a range of cut-off sizes. The observed differences in the spread are due to slightly higher vaporization rates in the peripherals of the mixing layer. Analysis shows that this is primarily due to above noted problem with the LES transport of the liquid phase. It is expected that the correction developed for this will result in more consistent predictions and will be reported at a future date.

Conclusions

Parallel simulations of unsteady turbulent combustion are performed for a range of precursor test problems leading to the development of a new methodology for reacting two-phase flows. All the relevant scales of interest in these problems can not be completely resolved even with the fastest available computers. Modeling in form of large-eddy simulations (LES) is advocated as a feasible solution. In LES, all scales larger than the grid size are computed exactly while the small scales are modeled. For two-phase applications, Lagrangian tracking is employed to follow the droplets and the effect of liquid phase is completely coupled to the gas phase equations. A subgrid model, which accurately accounts for small-scale scalar

mixing, chemical reactions and vaporization, is implemented on a one-dimensional domain contained within each LES cell. These subgrid computations in each LES cell are independent of other LES cells and thus making the procedure highly parallelizable. The LES code has been optimized to have minimum communication and I/O overheads. The results show a near linear scale-up in parallel efficiency upto 128 processors (CRAY T3E). Stagnation point premixed flame, opposed jet diffusion flame, highly swirling premixed flame in a General Electric combustor and two-phase mixing and vaporization in mixing layers are studied using this code. Comparison with experimental data, wherever possible, clearly demonstrates the unique capabilities of this highly-parallelizable subgrid-combustion LES approach.

Acknowledgments

This work was supported in part by the Army Research Office Multidisciplinary University Research Initiative grant DAAH04-96-1-0008 and by the Air Force Office of Scientific Research Focused Research Initiative contract F49620-95-C-0080, monitored by General Electric Aircraft Engine Company, Cincinnati, Ohio. Computations were carried out under the DoD HPC Grand Challenge Project at NAVO, Stennis Space Center and ARC, Huntsville.

References

Calhoon, W. H. and Menon, S. (1996) "Subgrid Modeling for Reacting Large-Eddy Simulations," AIAA 96- 0516, 34th AIAA Aerospace Sciences Meeting.

Calhoon, W. H. and Menon, S. (1997) "Linear-Eddy Subgrid Model for Reacting Large-Eddy Simulations: Heat Release Effects," AIAA 97-0368, 35th AIAA Aerospace Sciences Meeting.

Chakravarthy, V. K. and Menon, S. (1997) "Characteristics of a Subgrid Model for Turbulent Premixed Flames," AIAA 97-3331

Cheng, R. K. and Shepherd, I. G. (1991) "The Influence of Burner Geometry on Premixed Turbulent Flame Propagation," Combustion and Flame, Vol. 85, pp. 7-26.

Cho, P., Law, C. K., Herzberg, J. R., and Cheng, R. K. (1986) "Structure and Propagation of Turbulent Premixed Flames Stabilized in a Stagnation Flow," Twenty-first Symposium (international) on Combustion, pp. 1493-1499.

Kerstein, A. R., Ashurst Wm., T. and Williams F. A. (1988) "The Field Equation for Interface Propagation in an Unsteady Homogeneous Flow Field," Physical Review A, 37, pp. 2728-2731.

Kim, W.-W. and Menon, S. (1995) "A New Dynamic One-equation Subgrid-scale Model to Turbulent Wall-bounded Flows," AIAA 95-0356, 33rd AIAA Aerospace Sciences Meeting.

Lazaro, B. J. and Lasheras, J. C. (1992a) "Particle Dispersion in the Developing Free Shear Layer," J. Fluid Mech., Vol. 235, pp. 143-178.

Lazaro, B. J. and Lasheras, J. C. (1992b) "Particle Dispersion in the Developing Free Shear Layer," J. Fluid Mech., Vol. 235, pp. 179-221.

Ling, W., Chung, J. N., Troutt, T. R. and Crowe, C. T. (1997) "Numerical Simulation of Particle Dispersion in a Three-dimensional Temporal Mixing Layer," 1997 ASME Fluids Engineering Division Summer Meeting, Vancouver.

Liu, Y. and Lenze, B. (1988) "The Influence of Turbulence on the Burning Velocity of Premixed ch_4 - h_2 Flames with Different Laminar Burning Velocities," Twenty-Second Symposium (International) on Combustion, pp. 747-754.

Martin, J. E. and Meiburg, E. (1994) "The Accumulation and Dispersion of Heavy Particles in Forced Two- dimensional Mixing Layers. I. The Fundamental and Subharmonic Cases," Phys. Fluids, Vol. 6 (3), pp. 1116-1132.

Menon, S., McMurtry, P., and Kerstein, A.R. (1993) "A Linear Eddy Mixing Model for LES of Turbulent Combustion," in Large-Eddy Simulations of Complex Engineering and Geophysical Flows, (B. Galperin and S. A. Orszag, Eds.), Cambridge Univ. Press, pp. 278-315.

Menon, S. and Kim, W.-W. (1996) "High Reynolds number flow simulations using the localized dynamic subgrid-scale model," AIAA 96-0425, 34th AIAA Aerospace Sciences Meeting.

Menon, S. and Calhoon, W. (1996) "Subgrid Mixing and Molecular Transport Modeling for Large-Eddy Simulations of Turbulent Reacting Flows," Symposium (International) on Combustion, 26, pp. 59-66.

Metcalfe, R. W., Orszag, S. A., Brachet, M. E., Menon, S., and Riley, J. J. (1987) "Secondary Instability of a Temporally Growing Mixing Layer," J. Fluid Mech., Vol. 184, pp. 207-243

Menon, S. and Pannala, S. (1997) "Subgrid Modeling of Unsteady Two-Phase Turbulent Flows," AIAA 97-3117.

Nelson, C. C. and Menon, S. (1998) "Unsteady simulations of compressible spatial mixing layers," AIAA 98-0786

Pannala, S. and Menon, S. (1998) "Large Eddy Simulations of Two-Phase Turbulent Flows," AIAA 98-0163

Pocheau, A. (1994) "Scale Invariance in Turbulent Front Propagation," Physical Review E., 49, pp. 1109-1122

Poinsot, T. (1996) "Using Direct Numerical Simulations to Understand Premixed Turbulent Combustion," Symp. (Int.) on Combustion, 26, pp. 219-232

Smith, T. M. and Menon, S. (1998) "Subgrid Combustion Modeling for Premixed Turbulent Reacting Flows," AIAA 98-0242.

Overall Grid	# PEs	$T_{communication}$	$T_{compute}$	T_{total}
CRAY T3E (Secs)				
192 x 192	8	4.2506326e-02	0.5077792	0.550285526
	16	4.6510745e-02	0.2514651	0.297975845
	32	5.5333067e-02	0.1284368	0.183769867
256 x 256	8	5.6338131e-02	0.6976048	0.753942931
	16	5.3589024e-02	0.3463882	0.399977224
	32	7.0091270e-02	0.1753119	0.24540317
SGI ORIGIN 2000 (Normalized by T3E data)				
192 x 192	8	0.193	0.184	0.185
	16	0.160	0.170	0.169
	32	0.346	0.185	0.233
256 x 256	8	0.205	0.268	0.263
	16	0.171	0.227	0.219
	32	0.285	0.233	0.248
IHPC CLUSTER (Normalized by T3E data)				
192 x 192	8	2.654	0.892	1.028
	16	1.958	0.867	1.037
	32	3.262	0.896	1.609
256 x 256	8	2.923	1.151	1.284
	16	2.256	1.139	1.289
	32	3.395	1.214	1.837

Table 1: Timings for the 2D code on different parallel systems. Note that I/O timing is not included.

Overall Grid	# PEs	$T_{communication}$	$T_{compute}$	T_{total}
CRAY T3E (Secs)				
96x64x80	8	1.20985875	9.984778125	11.19463688
	16	0.687654344	5.030144063	5.717798406
	32	0.478368688	2.593220781	3.071589469
	64	0.337139852	1.355396953	1.692536805
	128	0.225933906	0.749989961	0.975923867
SGI ORIGIN 2000 (Normalized by T3E data)				
96x64x80	8	0.571	0.488	0.497
	16	0.553	0.460	0.471
	32	0.841	0.528	0.577

Table 2: Timings for the 3D LES code with one species (G eqn.) on different parallel systems. Note that I/O timing is not included.

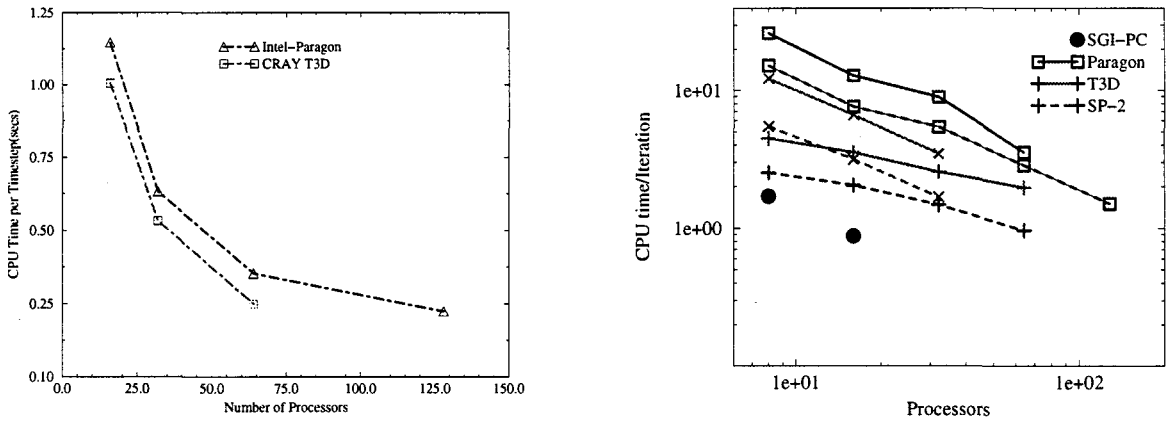

Figure 1: Scaling on different machines. (a) Axisymmetric code (with 6 scalars and chemistry), (b) 3-D code (dashed line-DNS with one scalar and solid line-LES with one scalar on a 96x64x64 grid)

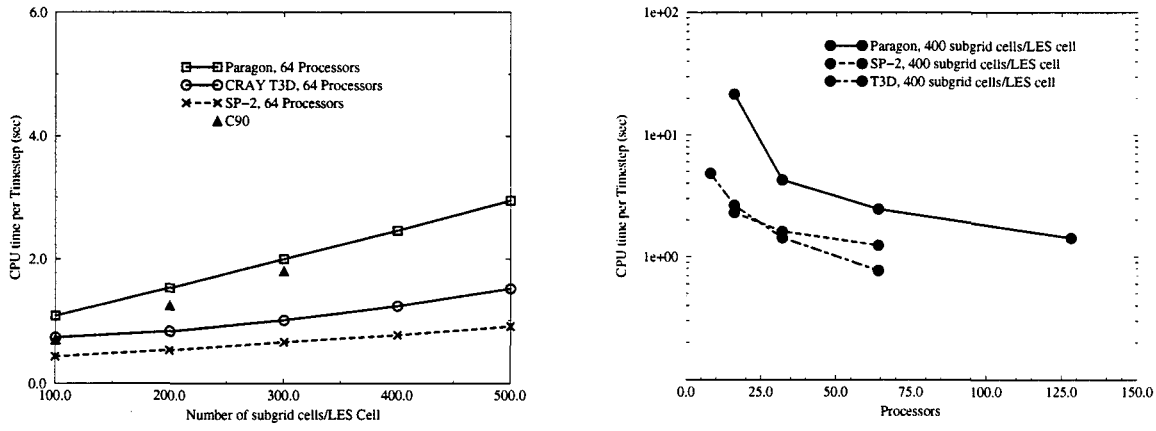

Figure 2: Performance with the new subgrid model. (a) Computation time by increasing the number of subgrid cells, (b) Scale-up on different machines with fixed number of subgrid cells

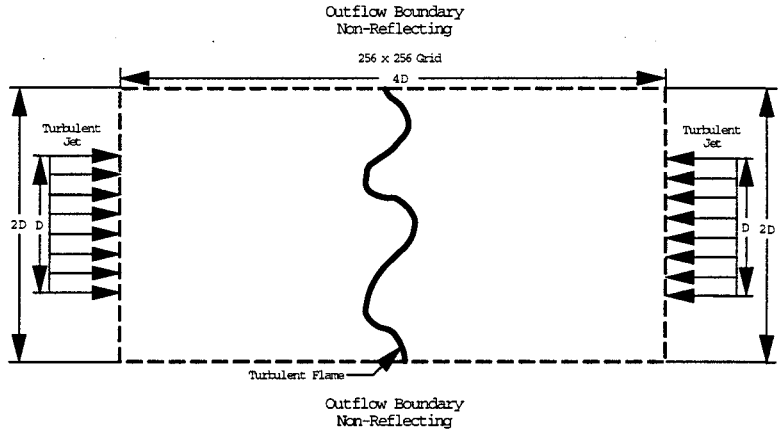

Figure 3: Set-up of the opposed jet diffusion flame

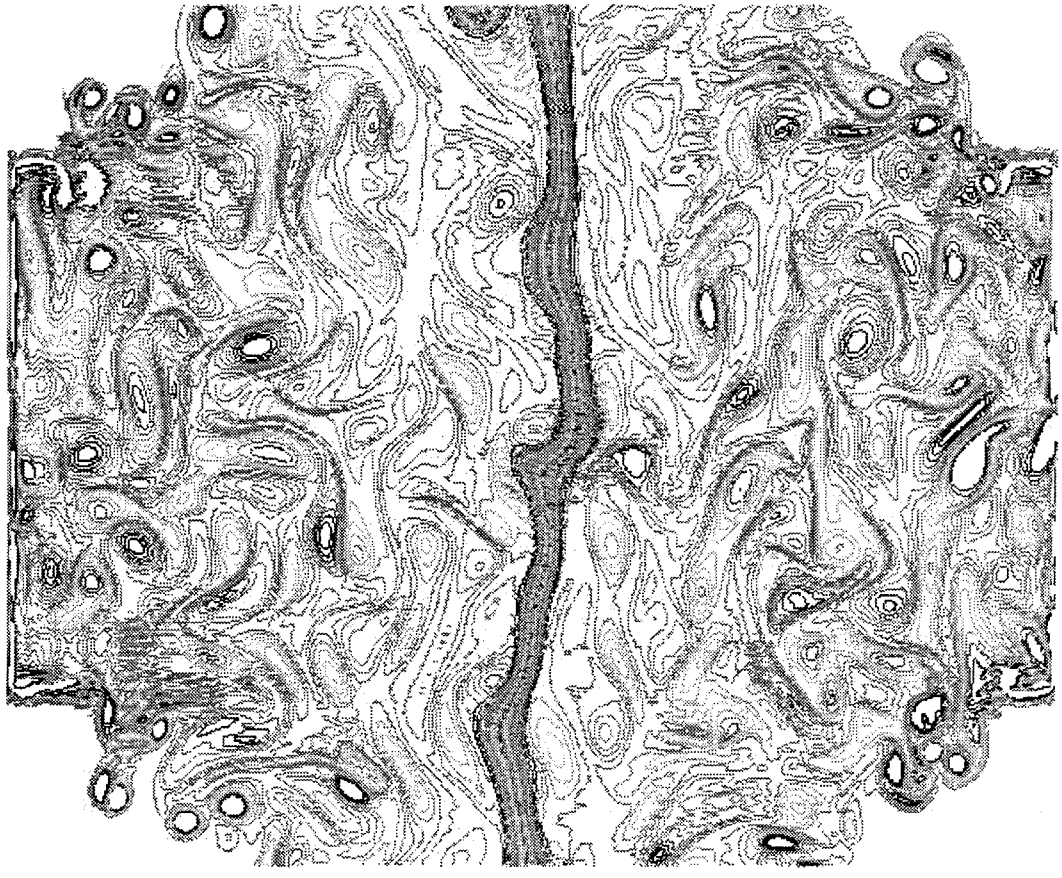

Figure 4: Typical vortex flame interaction in the opposed jet diffusion flame.

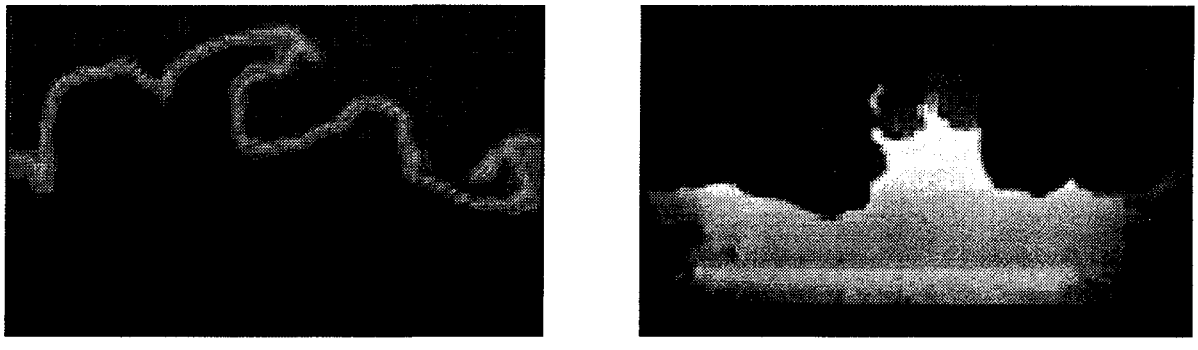

Figure 5: Instantaneous flame in a stagnation point flame. (a) LES and (b) Experiment (Cheng, LBNL)
Note: The flow is from bottom and the top plane corresponds to wall

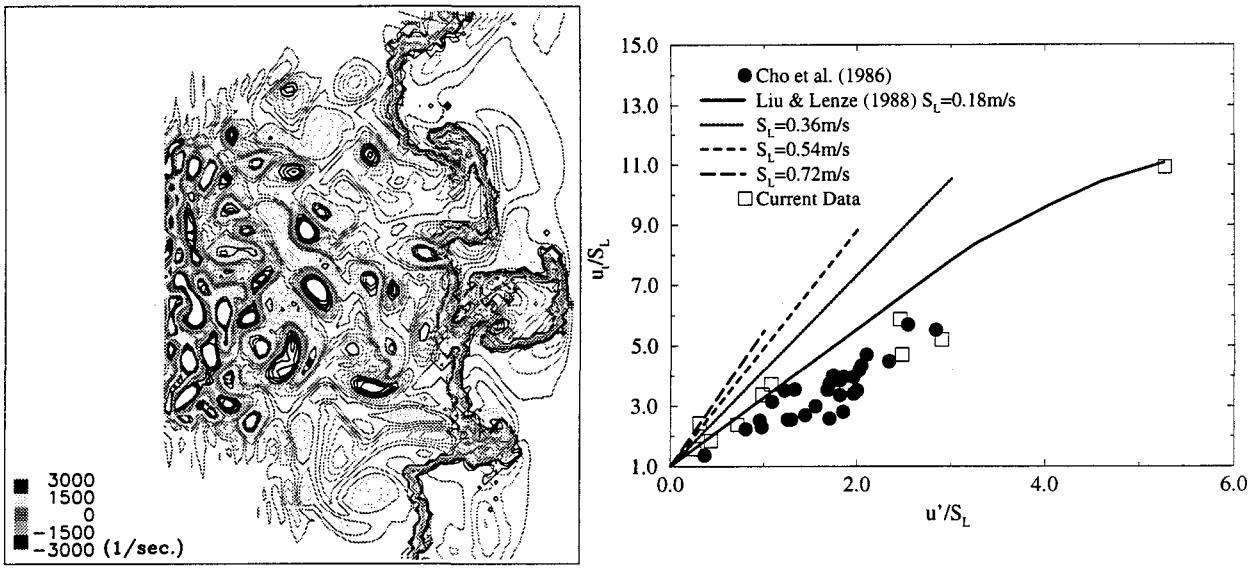

Figure 6: (a) Flame vortex interaction for S_L (Flame Speed) = 0.25m/s and T_p/T_f (ratio of product temperature to that of premixed temperature) = 4 and (b) Comparison of turbulent flame speed with experimental data. Predictions from simulations are compared to experimental data by Cho *et al.* (1986) and Liu and Lenze (1988).

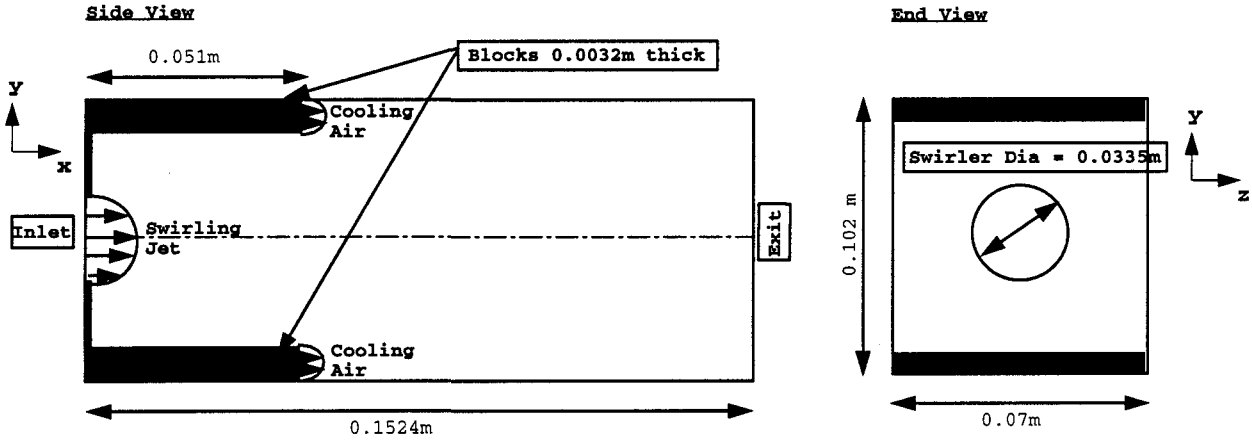

Figure 7: Schematic of the GE low NOx Premixed Combustor.

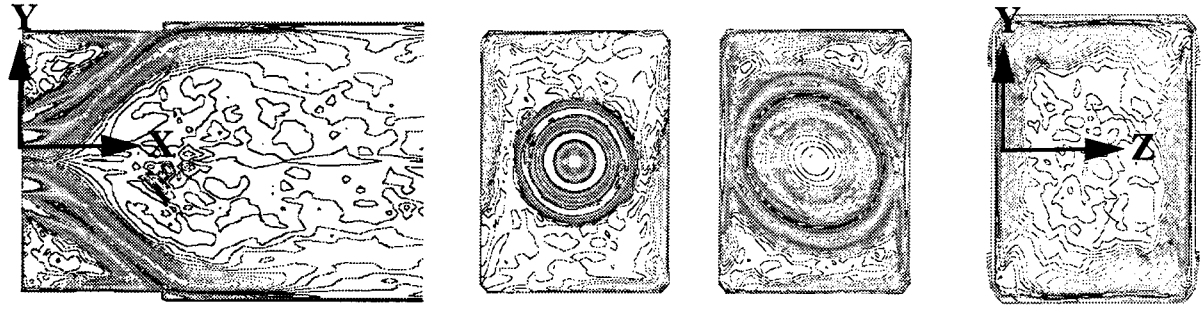

Figure 8: Averaged vorticity magnitude contours in the GE combustor. (a) Side view, (b) End view (x=6 mm), (c) End view (x=24 mm) and (d) End view (x=78 mm)

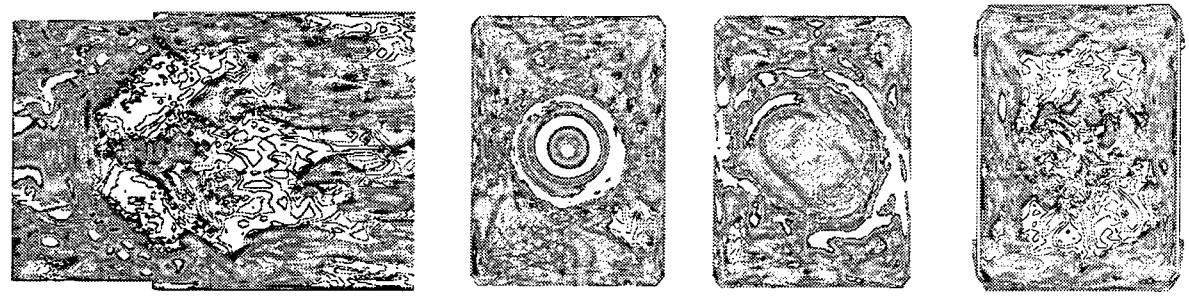

Figure 9: Instantaneous vorticity magnitude contours in the GE combustor. (a) Side view, (b) End view (x=6 mm), (c) End view (x=24 mm) and (d) End view (x=78 mm)

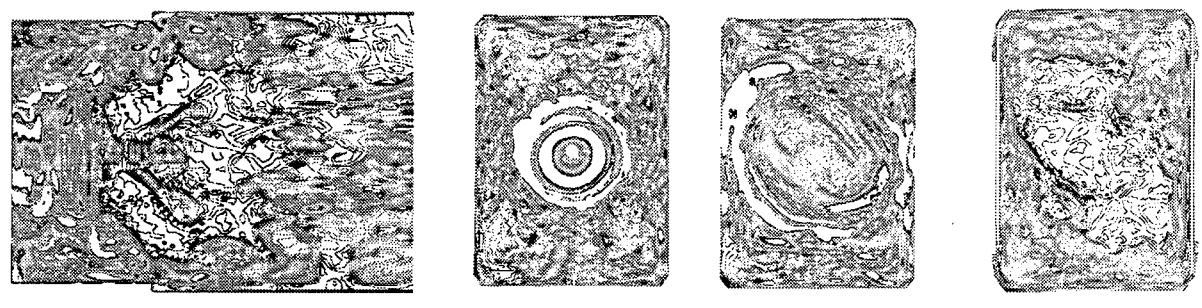

Figure 10: Instantaneous vorticity magnitude contours in the GE combustor. (a) Side view, (b) End view (x=6 mm), (c) End view (x=24 mm) and (d) End view (x=78 mm)

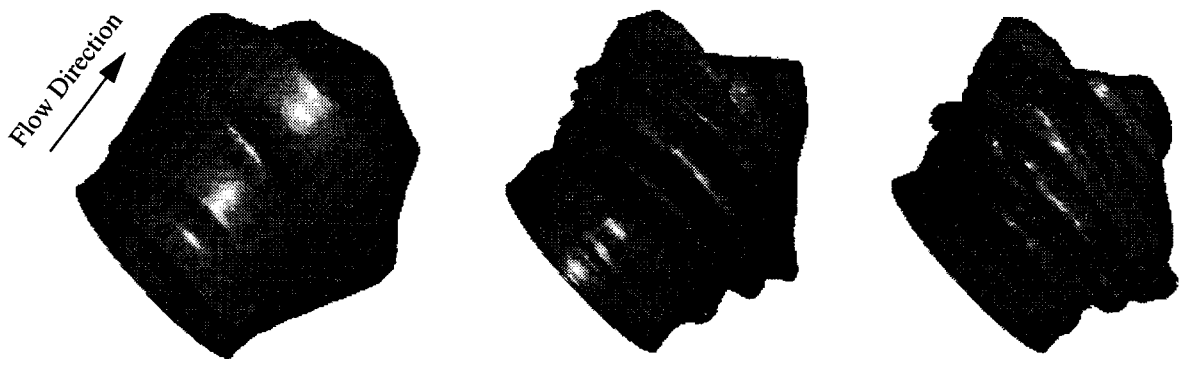

Figure 11: Flame kernel in the GE combustor (a) Time Averaged; (b) and (c) Two instantaneous snap shots.

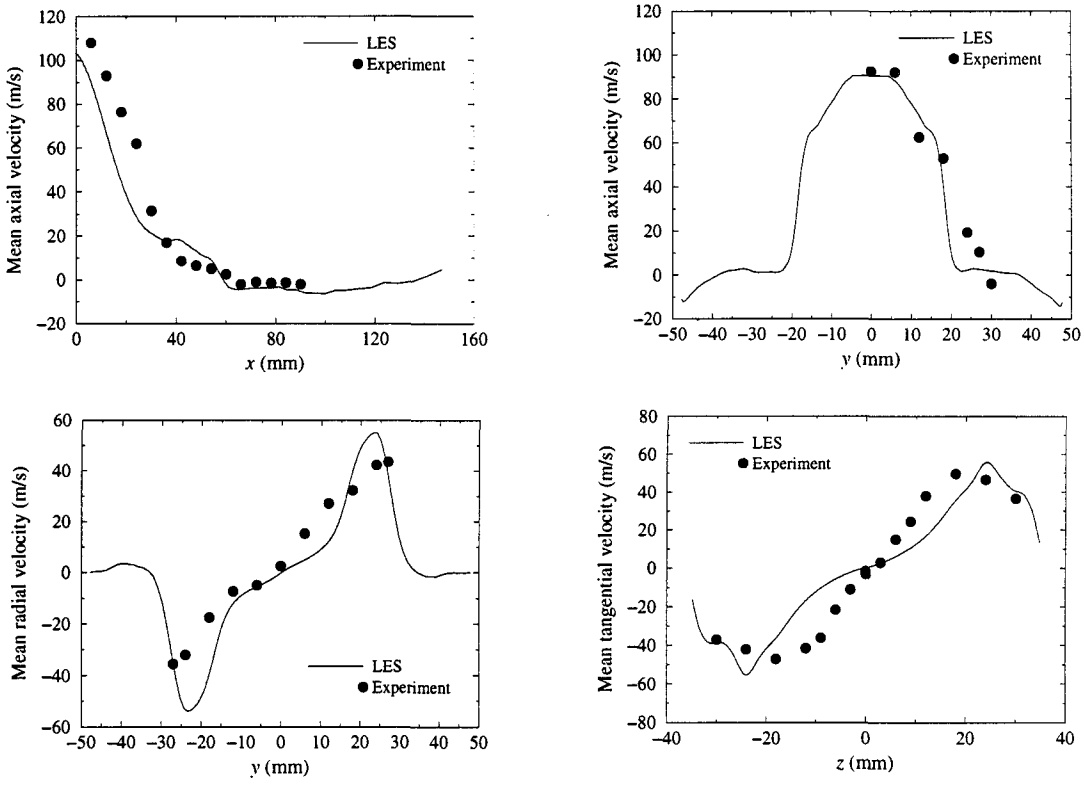

Figure 12: Variation of mean velocities in the GE combustor (a) Axial velocity along the combustor center line, (b) Lateral variation of axial velocity, (c) Lateral variation of radial velocity and (d) Lateral variation of tangential velocity.

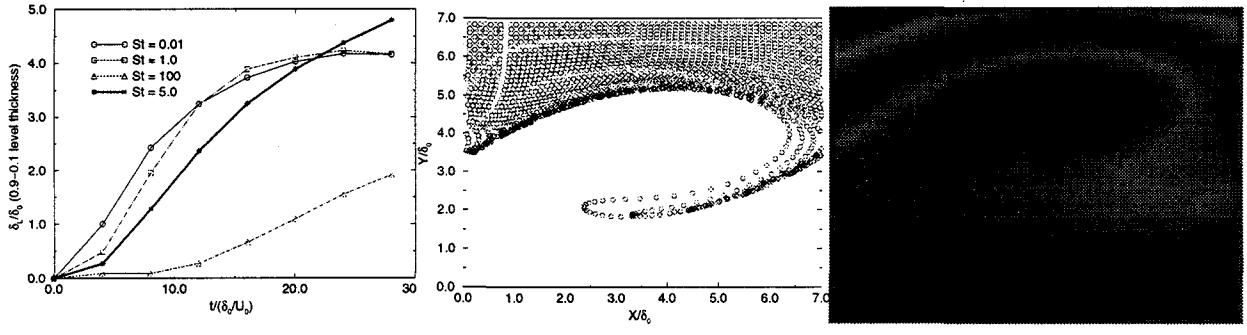

Figure 13: Particle dispersion in a 3-D mixing layer. (a) Evolution of 0.1-0.9 particle thickness for different stokes numbers, (b) Droplet distribution for St=5 showing the centrifuge effect and (c) Flash pulse visualization of Lazaro and Lasheras (1992b).

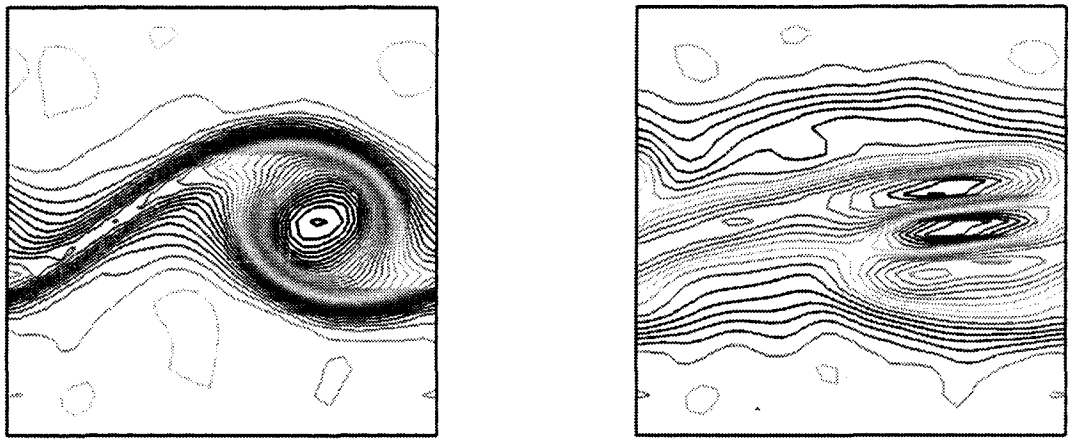

Figure 14: Spanwise vorticity in the mixing layer. (a) without liquid-gas coupling from droplets and (b) with liquid-gas coupling. Note: Contour interval level = 0.0374.

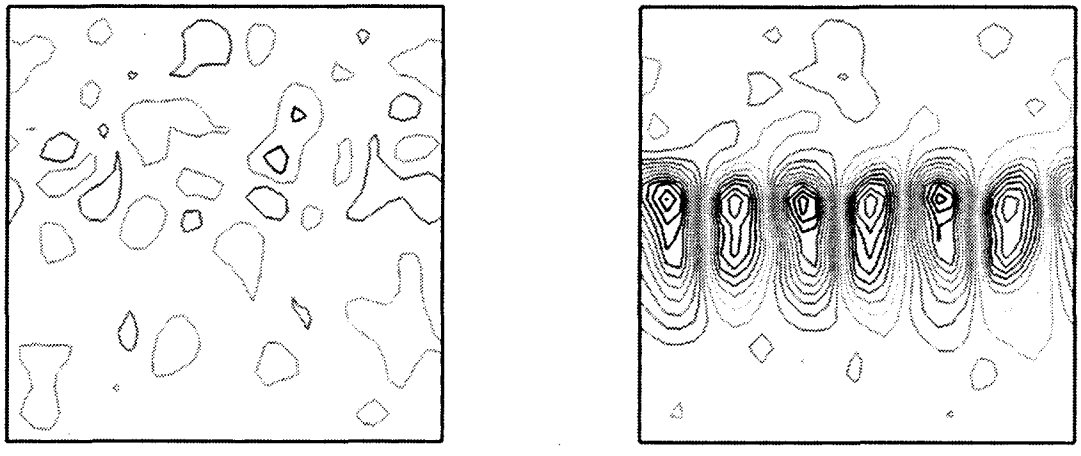

Figure 15: Streamwise vorticity in the mixing layer. (a) without liquid-gas coupling and (b) with liquid-gas coupling. Note: Contour interval level = 0.03

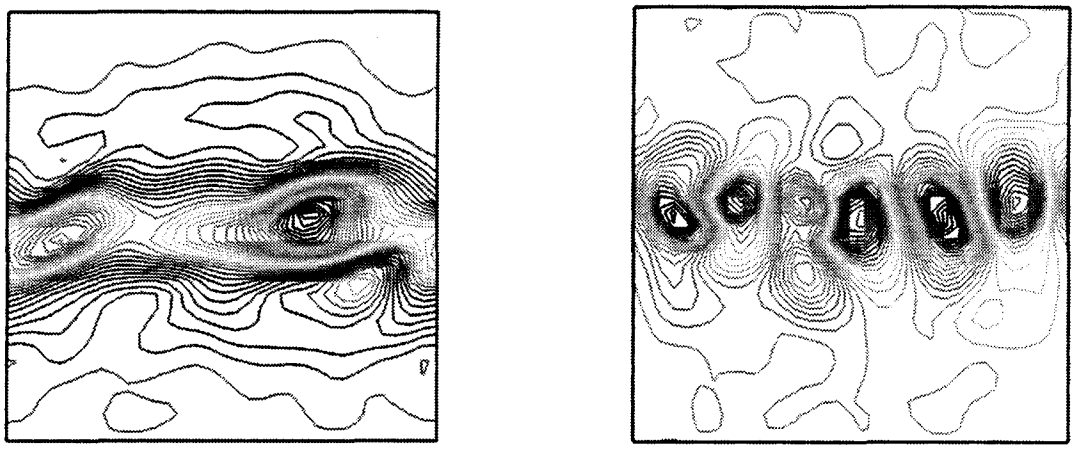

Figure 16: Variation across mixing layer using 2-phase LES/LEM methodology. (a) Spanwsie vorticity (contour interval = 0.0374), (b) Streamwise vorticity (contour interval = 0.03)

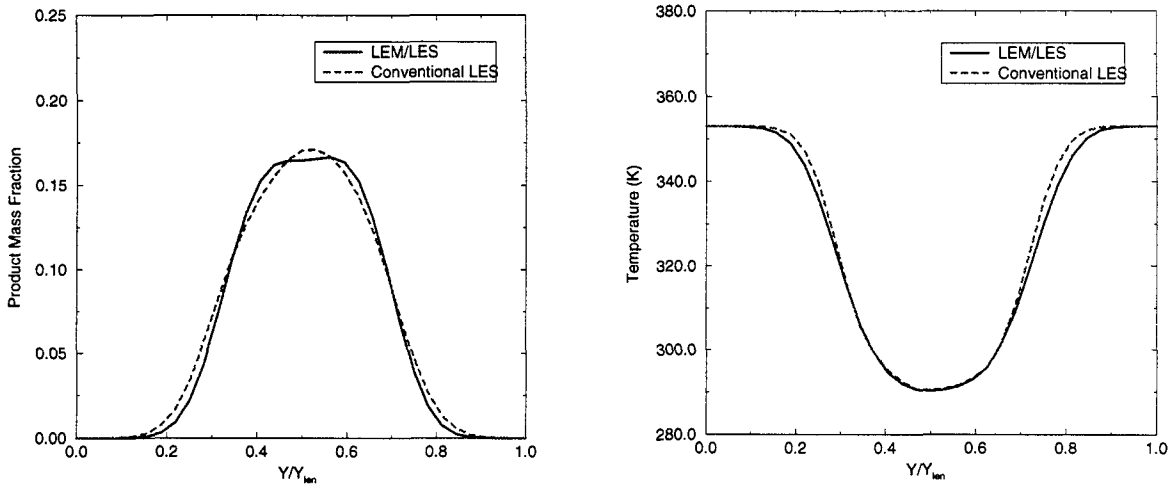

Figure 17: Comparison of conventional and current methodology. (a) Variation of product mass fraction across the mixing layer and (b) Variation of temperature across the mixing layer.

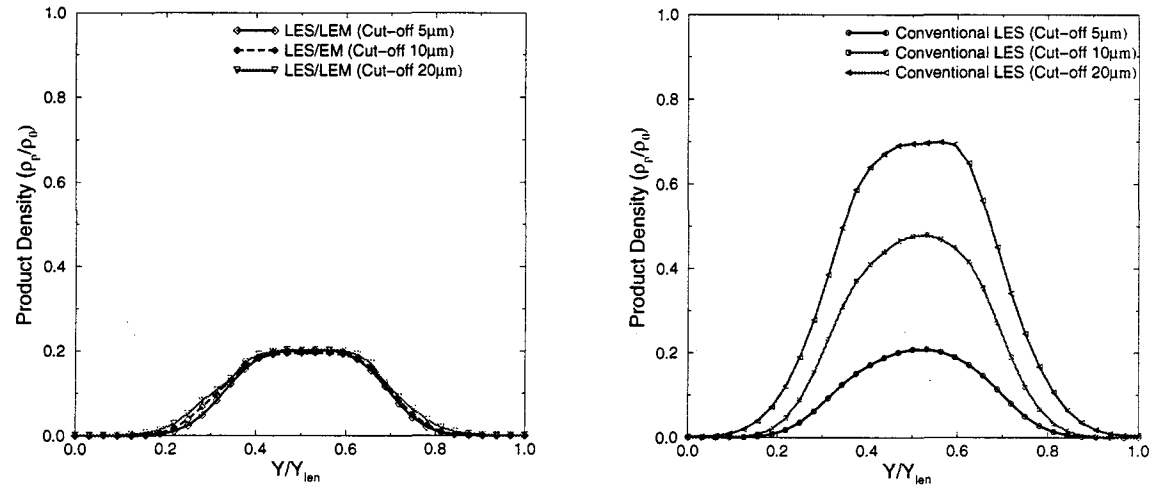

Figure 18: Comparison of the two methods in predicting product density across the mixing layer for different cut-offs. (a) LEM/LES and (b) Conventional LES.